Eur Biophys J (1998) 27: 105–112

ARTICLE

Wei Cheng · Cun Xin Wang · Wei Zu Chen
Ying Wu Xu · Yun Yu Shi

Investigating the dielectric effects of channel pore water on the electrostatic barriers of the permeation ion by the finite difference Poisson-Boltzmann method

Received: 28 January 1997 / Accepted: 24 September 1997

Abstract In this paper, the finite difference Poisson-Boltzmann (FDPB) method with four dielectric constants is developed to study the effect of dielectric saturation on the electrostatic barriers of the permeation ion. In this method, the inner shape of the channel pore is explicitly represented, and the fact that the dielectric constant inside the channel pore is different from that of bulk water is taken into account. A model channel system which is a right-handed twist bundle with four α-helical segments is provided for this study. From the FDPB calculations, it is found that the difference of the ionic electrostatic solvation energy for wider domains depends strongly on the pore radius in the vicinity of the ion when the pore dielectric constant is changed from 78 to 5. However, the electrostatic solvation energy of the permeation ion can not be significantly affected by the dielectric constant in regions with small pore radii. Our results indicate that the local electrostatic interactions inside the ion channel are of major importance for ion electrostatic solvation energies, and the effect of dielectric saturation on the electrostatic barriers is coupled to the interior channel dimensions.

Key words Pore constant · Electrostatic barrier · The FDPB method

W. Cheng [1] · Y. Y. Shi
Department of Biology,
University of Science and Technology of China,
Hefei, Anhui 230026, P. R. China

C. X. Wang (✉) · W. Z. Chen · Y. W. Xu
Center for Fundamental Physics,
University of Science and Technology of China,
Hefei, Anhui 230026, P. R. China
(e-mail: xin@iris.bio.ustc.edu.cn)

Present address:
[1] Department of Biochemistry and Molecular Biophysics,
Washington University, School of Medicine,
St. Louis, MO 63110, USA

Introduction

The effect of dielectric saturation inside the ion channel on the electrostatic barriers of the permeation ion is, both theoretically and experimentally, a very important issue. In conventional studies, the dielectric constant of the aqueous pore has been considered as a high value (~80). This means that pore water and bulk water are dielectrically equivalent, and the associated permeation free energy barriers are low enough to be consistent with kinetic data (Parsegian 1969; Levitt 1978). However, recent analysis demonstrates that high values of the dielectric constant are not consistent with the more realistic description of pore water. The properties of the water molecules within the channel pore have been proposed to the different from those of bulk water (Partenskii and Jordan 1992; Breed et al. 1996). Both the translational and rotational mobility of water molecules inside the channel pore seem to be reduced relative to those of bulk water (Breed et al., 1996). When the ion is present in the channel, dielectric saturation will occur and the dipole polarization of water molecules will be reduced. The direct result of the dielectric saturation is the reduction of the water dielectric constant.

It has been proposed that both the structure and charge distributions in the channel pore contribute to electrostatic influences on channel conductance (Jordan 1986). On the basis of this consideration, it is improper to deal with the long-range interactions with simplified channel models such as a cylinder or other geometry. The goal of the present work is to study how the dielectric saturation affects the electrostatic solvation energy of the permeation ion. The FDPB method (Sharp and Honig 1990) is used to calculate the electrostatic solvation energy for a model channel system. In this method, the detailed shape of the inner pore is incorporated into electrostatic solvation energy calculations so that the dielectric response of the water molecules inside the channel pore can be separately treated with dielectric constants which are different from that of bulk water. In our model system, the lipid bilayer is also included and treated with a dielectric constant of 2.

In the present study, a 22-mer peptide which mimics the sequence of S3 segments of the voltage-sensitive sodium channel has been selected as our model system because of its reasonableness and relative simplicity, as well as because of the physiological importance of the model. Previous experimental and simulation studies (Oiki et al. 1988; Greenblatt et al. 1985) have suggested that such a 22-mer peptide would form a transmembrane ion channel structure with a bundle of four amphipathic α-helices in lipid bilayers. From recent experimental NMR work (Doak et al. 1996), it has also been demonstrated that synthetic peptides dissected from the rat brain II sodium channel that share high homology with our model peptide are predominantly α-helical in trifluorethanol and in dodecylphosphocholine micelles. However, it should be noted that the channel activity of this peptide in lipid bilayers may not have any relationship to the conductance properties of intact Na^+ channels (Stephan and Agnew 1991). Since the main interest of this work is to study the dielectric behavior of channel pore water other than the conductance properties of the ion, our model system of the S3 peptide is suitable for this study with the theoretical FDPB method.

The outline of the paper is as follows. The procedures to build the channel model and the methods for separating the aqueous pore into the different regions for the FDPB calculation are described in the next section. Then, our results obtained from the FDPB calculations are reported and discussed. Finally, some important points are summarized in the conclusions.

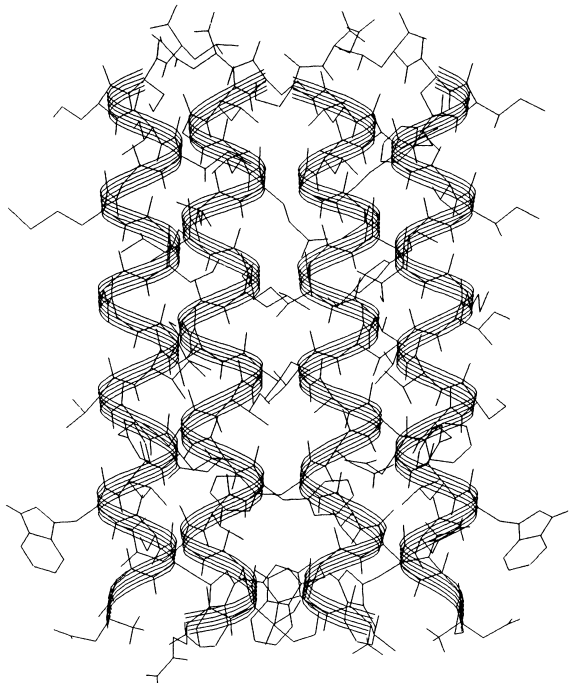

Fig. 1 The initial structure of the channel model in which helices are exactly parallel to each other

Model and computational details

Channel model building and simulation procedures

The model channel was built with the INSIGHT II package from Biosym Technologies. The 22-mer peptide sequence, DPWNWLDFSVVTMTYITEFIDL, was taken according to Greenblatt et al. (1985), and mimicked the S3 region of the voltage-sensitive sodium channel. In the beginning, the four segments of the channel model were separately constructed using idealized α-helices, in which the spacing distance between residues is taken as 0.15 nm and each turn includes 3.6 residues. Then, the four segments were combined to form an initial channel structure of a bundle with an exactly parallel helix tetramer (shown in Fig. 1). The N-terminus of the model was assigned to the intra-cellular side of the membrane (Greenblatt et al. 1985). The structural model of Noda et al. (1986) was selected as our reference to construct the channel pore. The acidic Asp residues in each helix were placed so as to face the inner pore of the channel.

In the present work, we used several different methods to study the packing of α-helices. In order to obtain a reasonable channel structure, we employed the simulated annealing (SA) procedure in the restraint molecular dynamics (MD) simulation to explore the equilibrium conformation of the model channel system (Nilges and Brünger 1991; Treutlein et al. 1992; Kerr et al. 1994). The GROMOS package (van Gunsteren and Berendsen 1987) was used for all MD simulations. After energy minimization (EM) of the initial structure, the temperature of the system was assigned at 500 K and a 30 ps MD simulation was performed for system equilibrium. Then, the system was cooled down to 300 K in step of 10 K followed by 1.25 ps MD equilibrium. When the temperature was reduced to 300 K, the restraints for the Cα atoms were gradually relaxed and a 30 ps MD simulation with constant temperature was performed followed by a 200 step steepest descent EM. The intra-helix distance restraints between the carbonyl atom O of residue i + 4 and the amide atom H of residue i were used to maintain α-helical geometry during all the MD simulations. The target distance for these restraints was derived from α-helical hydrogen-bonding geometries observed after EM. During the last 30 ps MD simulation, if the distance between the termini of two helices exceeded the target value, a new distance restraint between the termini of the helices was applied to prevent the monomers from moving too far apart. It is worth noting that this distance restraint can leave the monomers free to rotate around their respective helix axes and no restraint was imposed on the angle between two helices. As shown in Fig. 2, though the helix bundles could take a left-handed twist or right-handed twist, the distances between two neighboring termini were still kept unchanged.

The system was then centered in a rectangular box of $8 \times 2 \times 2$ nm^3 with 715 SPC water molecules (Berendsen et al. 1981). After removing the water molecules that were too close to the channel atoms, the system contained 613

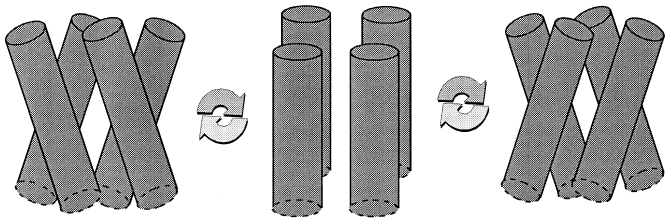

Fig. 2 Schematic illustration of the effect of the termini distance restraint during MD simulations at 300 K. The distance between neighboring helices is restrained. The helix bundle can take a left-handed twist or a right-handed twist without changing the restrained distance

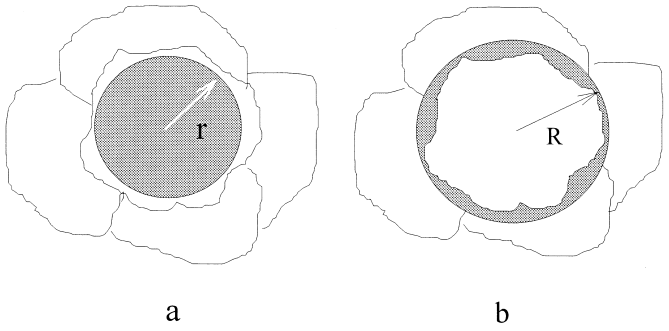

Fig. 3a, b Schematic representation of the irregular surfaces of the channel pore: **a** the sphere obtained from the program HOLE is plotted as the dark circular region with radius r, and the cavities of the internal surfaces are not considered in the sphere; **b** the circle with radius R obtained from the program PORE is represented by the dark circular region, and the cavities of the internal surfaces are considered in this region

water molecules. A further check of the system showed that no water molecules were in contact with the presumed lipid-facing surfaces of the helix bundle. Then, a 70 ps full MD simulation with position restraints for all Cα atoms was carried out at 300 K to provide an equilibrium system. The SHAKE algorithm (Ryckaert et al. 1977) was used to constraint bond lengths in EM and MD simulations. The temperature was kept constant by coupling the system to a thermal bath (Berendsen et al. 1984) with temperature relaxation time 0.01 ps for the starting 500 steps and 0.1 ps for the remaining MD simulation. A force constant of 1,000 kJ $\cdot$ mol^{-1} $\cdot$ nm^{-2} was used for distance restraint. The non-bonded forces were calculated with the twin-range charge group technique (van Gunsteren and Berendsen 1987) with cuf-offs of 1 nm, and the neighbor pair list was updated every 10 steps.

The dielectric constant assignment for the channel model

In the normal FDPB method, a two-dielectric continuum model was used, in which the solvated protein was represented as a uniform low dielectric solute surrounded by a continuum of high dielectric solvent. Since the water molecules in the channel pore have different properties from those in the region of bulk water, the channel protein and its aqueous pore need to be carefully considered. Therefore, our basic idea was to circumscribe the channel pore with its detailed shape and the dielectric constants were treated separately from those of bulk water. The procedure included mainly the following two parts.

First, the inner dimensions of the channel pore were evaluated. The program HOLE reported by Smart et al. (1993) can be used to provide the channel pore dimensions. In the program HOLE, the Monte Carlo SA procedure (Metropolis et al. 1953; Kirkpatric et al. 1983) was used to produce a series of spheres along the channel axis, which do not overlap any protein atoms. We have found that although the program HOLE is effective to get the inner size of the channel pore, the problem is that the cavities of the internal surface in the channel are neglected owing to the irregular shape of the internal surface (see Fig. 3a). As far as the long-range electrostatic effects are concerned, these inner cavities should be considered in the calculation. Therefore, we developed a program PORE to overcome this deficiency, in which the SA algorithm similar to the program HOLE was used to generate a series of circles perpendicular to the channel axis. The displacement for a Monte Carlo step was set to 0.01 nm. The centers of all circles were located at the channel axis, and those circles can completely cover the aqueous pore with the least overlapping of the channel protein atoms (see Fig. 3b).

Second, the pore dimensions were incorporated into the FDPB calculation. Using the centers and radii of the all circles obtained from the program PORE, a cylinder with a defined radius can accommodate all these circles. The detailed method to search for the cylinder is given in the Appendix. With the defined cylinder, the dielectric constant for the FDPB calculations can be assigned. Figure 4 shows the schematic representation for the dielectric constant assignment. In the first step, the dielectric constants were assignment to each grid point according to whether the grid point was within the sphere of the van der Waals radius of channel protein atoms. The solvent probe radius was also considered in this step. The second step was to separate the channel pore from the rest of the grid. The grid points inside the channel pore were all assigned a new value of the dielectric constant, and the water molecules outside the channel were assigned the dielectric constant of bulk water. Therefore, the detailed shape of the aqueous pore was explicitly separated with the cylinder.

To guarantee a continuous change of the water dielectric constant, $\varepsilon_{\mathrm{pw}}$, along the channel axis z, a dielectric function for the water dielectric constant in the channel pore region (Daggett et al. 1991) is given by

$$\varepsilon_{pw} = \begin{cases} e^{z}\,(a_1 z^2 + b_1 z + c_1) + d_1 \\ \text{for} \quad z_{\min} < z < z_{\min} + 5 \\ \varepsilon_{pw0} \\ \text{for} \quad z_{\min} + 5 < z < z_{\max} - 5 \\ e^{z}\,(a_2 z^2 + b_2 z + c_2) + d_2 \\ \text{for} \quad z_{\max} - 5 < z < z_{\max} \end{cases}, \tag{1}$$

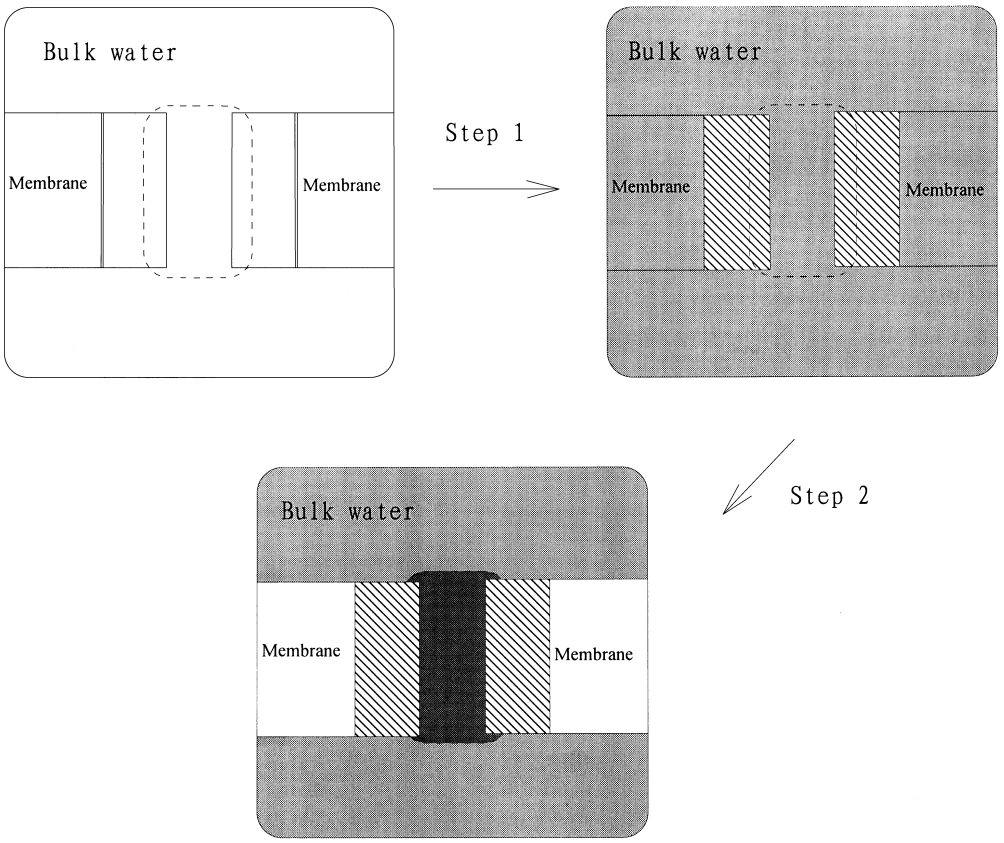

Fig. 4 Schematic representation of the dielectric constant assignment to the finite difference grid before solving the Poisson-Boltzmann equation. The defined cylinder is shown with the dashed lines. Step 1 and step 2 show the assignment procedures. In step 2, the model system is separated into four different regions: the thin line region is for the channel model, the dark black region for the water pore, the white region for membrane lipid, and the grey region for bulk water

where z is the atom coordinate in the direction of the channel axis (in Angstroms), z_{min} and z_{max} are the minimum and maximum value of *z*, and ε_{pw0} is referred to as the pore dielectric constant which can be given in the input parameter file. All eight parameters (a_1, b_1, c_1, d_1, a_2, b_2, c_2, d_2) in Eq. (1) can be calculated according to the following eight equations: $\varepsilon_{pw}(z_{min} + 5) = \varepsilon_{pw}(z_{max} - 5) = \varepsilon_{pw0}$, $\varepsilon_{pw}(z_{min}) = \varepsilon_{pw}(z_{max}) = 78$, $\varepsilon'_{pw}(z_{min}) = \varepsilon'_{pw}(z_{min} + 5) = 0$ and $\varepsilon'_{pw}(z_{max}) = \varepsilon'_{pw}(z_{max} - 5) = 0$, in which the symbol $'$ represents the derivative of the function. This means that there are maximum values of 78 for ε_{pw} at z_{min} and z_{max} and minimum values for ε_{pw0} at $z_{min} + 5$ and $z_{max} - 5$, respectively. In addition, the influence of the lipid bilayer in our model on the electrostatic interactions was considered by using a low dielectric constant of 2.

Calculation of the electrostatic solvation energy of the permeation ion

According to Sharp and Honig (1990), the electrostatic free energy of a collection of charges q_i in the system, E_{elec}, can be written as

$$E_{elec} = \frac{1}{2}\sum_i q_i \Phi_I, \tag{2}$$

where Φ_I is the total potential at the ith charge and contains contributions from electronic polarizability, solvent screening and mobile ions if they are present. The value of Φ_I can be obtained from the FDPB calculation. The electrostatic enery in vacuo was taken as the reference state. The change in electrostatic energy upon transfer of a solute molecule from one medium to another defines the electrostatic solvation energy. From Eq. (2), when the pore dielectric constant ε_{pw0} in Eq. (1) is changed, the electrostatic solvation energy difference, ΔE, is given by

$$\Delta E = \frac{1}{2}\sum_i q_i \Delta\Phi_I, \tag{3}$$

where $\Delta\Phi_I$ is the change in potential Φ_I due to the change in pore dielectric constant.

The atom coordinates of the channel model were taken from the structure obtained from the last 70 ps MD simulation in water. The values of atom charges were taken from the GROMOS force field. The inwardly facing Glu and Asp residues have been assumed to be in their fully deprotonated state. The ion was treated as a point charge within a dielectric sphere with the dielectric constant of 2 and placed inside the channel. The dielectric constant for the peptide helix was set to 4 to mimic the dipole reorientation effect. The dielectric constant for bulk water was set to 78. The dielectric constant for pore water can be determined with Eq. (1). The low ionic strength of 0.093 M was taken into account so that the linear Poisson-Boltzmann equation was enough to get accurate results in the FDPB calculation (Jordan et al. 1989). The 400 iteration steps

were performed for each solution. A two-step focusing technique was used to obtain better results (Gilson et al. 1987). In the first run, the molecule was scaled to occupy 61% of the lattice, and the zero boundary conditions for the potential were used. In the second run, the channel was scaled to occupy 92% of the lattice so as to obtain finer grids, and the potential map obtained from the first run was used. In all FDPB calculations, the lattice order was 65. The molecular surface was defined with a 0.14 nm probe radius. The cavity radius for the sodium ion was set to 0.168 nm according to Rashin and Honig (1985). Throughout this work, energies are expressed in kcal/mol, and charges in units of electron charge.

Results and discussion

The structure of the channel model

The SA/MD method has become a reliable technique for identifying the low-energy packing arrangements of α-helices (Nilges and Brünger 1991). In the current study, SA/MD is used to generate a rational channel model formed by parallel α-helix bundles. The final structure of the ion channel model obtained from MD simulation, shown in Fig. 5, is a right-handed twist bundle. The pore dimensions provided from the program PORE as a function of the distance along the channel axis are plotted in Fig. 6a–c. From Fig. 6a, it is found that there is a fairly large change in the local pore dimensions of the structure

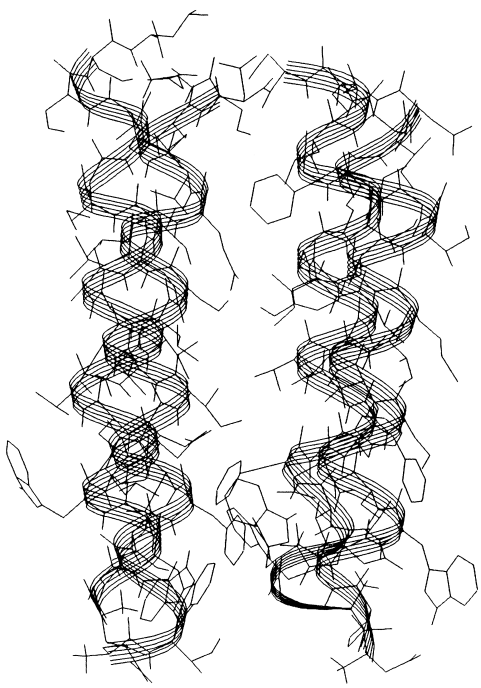

Fig. 5 The final channel structure with the right-handed twist bundle

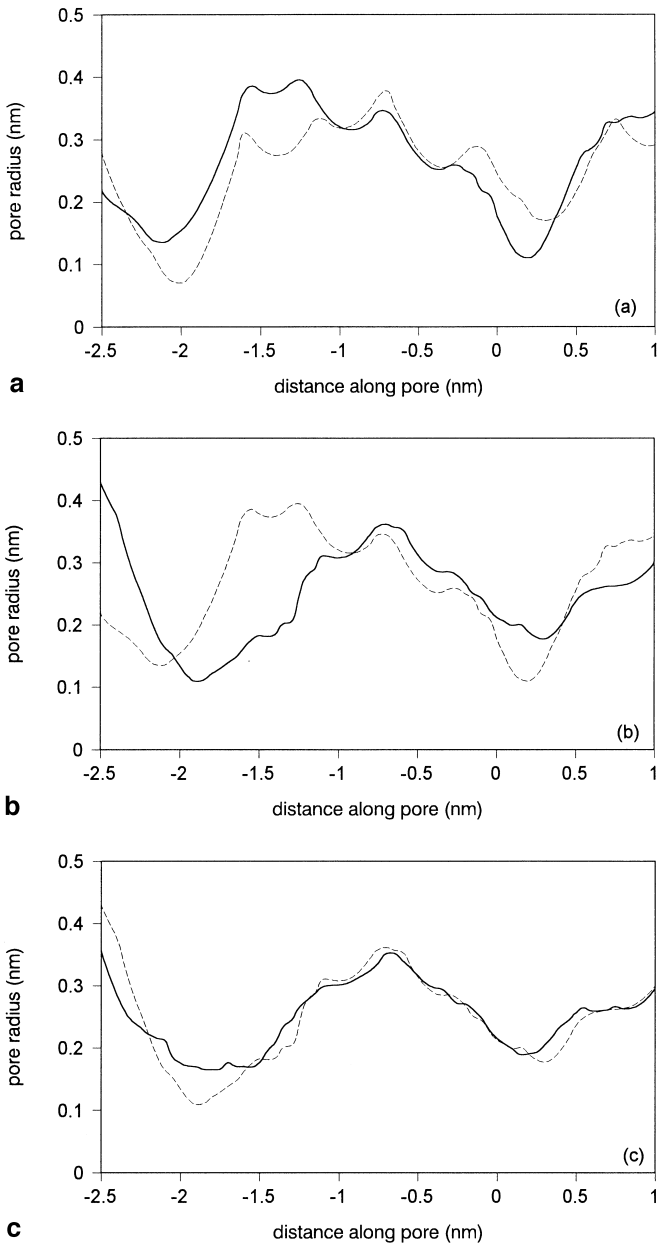

Fig. 6a–c Channel pore dimension versus the distance along the channel axis (in nm) is plotted for comparisons between different structures: **a** the *solid line* represents the structure after EM and the *dashed line* refers to the initially built structure; **b** the *solid line* represents the structure obtained from SA/MD simulation in vacuo and the *dashed line* is for the structure after EM; **c** the *solid line* represents the structure after MD equilibrium with explicit water and the *dashed line* is for the structure obtained from SA/MD simulation in vacuo

after EM compared with the initial structure. It appears that the EM is effective in reducing the unfavorable interactions among inner side chains. As shown in Fig. 6b, more drastic dimension changes are observed after the SA/MD simulation in vacuo as the system is annealed from 500 K and then equilibrated at room temperature. However, when

the MD simulation with explicit water is carried out, the pore dimensions are very similar to those obtained from the SA/MD simulation in vacuo (see Fig. 6c). It can be deduced that the inner side-chain conformation obtained from the SA/MD simulation in vacuo is a quite stable one. Though a number of water molecules are included in the system, these water molecules do not have a significant influence on the side chain conformations.

It has been proposed that a left-handed twist is a favored by the non-bonded interactions among helices (Chothia 1984; Chou et al. 1988). To examine the rationality of the right-handed twist structure obtained from our simulation, we have also performed a global search for both right-handed and left-handed twist structures, and the results all show the energetic superiority of the right-handed bundle. Actually, it is worth noting that a variety of positive and negative values of twist angles has been found in crystal structures (Chothia et al. 1977; Richmond and Richards 1978). Using SA/MD modeling, Treutlein and co-workers (1992) have also got a super-coiled structure with a right-handed twist for transmembrane peptides. It has been proposed that for α-helical bundles, the side-chain interactions, especially the hydrophobic side-chain interactions on the exterior of the bundle, are the dominant factors of the twist angle (Sansom 1993; Sansom and Kerr 1993). Therefore, we suggest that the amino acid sequence is very important in defining the twist of helix bundles as it determines the characters of side chains, and the right-handed twisted bundle presented in this work may be reasonable because of its specific sequence.

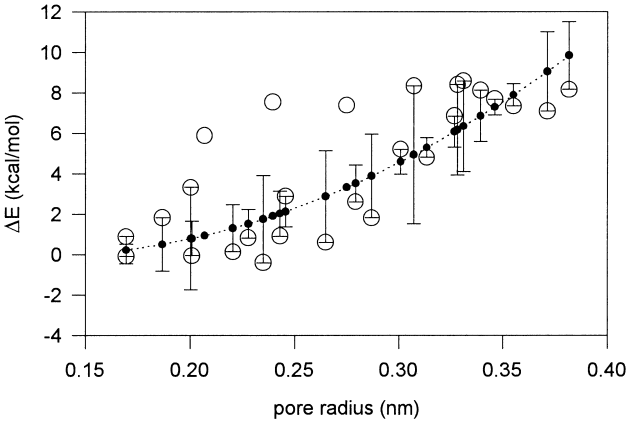

Fig. 7 The electrostatic solvation energy difference of the ion, ΔE, is plotted versus the local pore radius when the pore dielectric constant varies from 78 to 5 (shown in *hollow circles*). The *dotted line* shows the fitted curve obtained from the quadratic curve fitting for the data points with a quadratic equation ($y = 148.9x^2 - 36.734x + 2.168$). The *small solid circles* and *error bars* represent the fitted data and the associated deviations for each fitted point, respectively

Dielectric effects of pore water

Different dielectric constants for water within the channel pore have been suggested in previous studies. For porin-like channels, a dielectric constant of 24 has been suggested (Gutman et al. 1992). However, for gramicidin-like channels, a dielectric constant ranging from 2.5 to 5 has been recommended (Partenskii et al. 1994). As the pore radius for our channel can be readily compared with that of gramicidin, a dielectric constant of 5 for the pore water was chosen for our calculation.

The electrostatic solvation energy differences of the permeation ion, ΔE, can be calculated with Eq. (3). Figure 7 shows the values of ΔE as a function of the local pore radius when the pore dielectric constant is changed from 78 to 5. From Fig. 7, it is found that the values of ΔE depend strongly on the local pore radius. The exists a quadratic curve correlation between ΔE and pore radius except for a few points. For instance, there are 3 points where the error bars are not marked in Fig. 7 since they are automatically excluded during the data fitting because of large deviation errors. However, the correlation appears to be good for most points. In the regions for the small local dimensions, the values of ΔE are also modest. This indicates that the electrostatic solvation energy of the permeation ion in the regions for smaller pore radii is changed less compared with the regions for larger pore radii when the pore dielectric constant is decreased from 78 to 5. According to this result, we suggest that the ion electrostatic solvation energy is largely determined by the local environment in these regions. The ion-water interactions in regions with smaller pore radii could be a minor part of the ion solvation energy but the electrostatic interactions between the permeation ion and the channel atoms in the vicinity of the ion are the dominant part. In contrast, it is also clear form Fig. 7 that the value of ΔE can exceed 8 kcal/mol for the wide domains. This indicates that the dielectric screening effects of water molecules have become significant for the wide domains. The larger the local pore dimensions, the stronger the dielectric effects of the channel pore water. In other words, more water molecules can be held in the wide domains so that the ion has more opportunity to interact with water molecules. Therefore, many electrostatic interactions between ion and channel protein atoms could be diminished due to the screening by these water molecules. In this case, the mobility of water molecules in the regions of the wide domains is also less restrained, which should result in their better ligation with the permeating ion. Since the properties of local water molecules in the large pore region become the major factor of the electrostatic solvation energy, the dramatic electrostatic energy difference could be revealed by the pore dielectric constant.

Though the pore dimension is a significant factor in ion solvation, the local charge distribution in the channel protein is also important. For instance, at the position where the interactions between water and the channel atoms are unfavorable, the actual solvation of the permeating ion by water molecules will be poor, even though the pore dimensions are large enough to have better ion solvation. This is why a few points in Fig. 7 deviate from the fitted curve. Given the result that most of the points in Fig. 7 are close

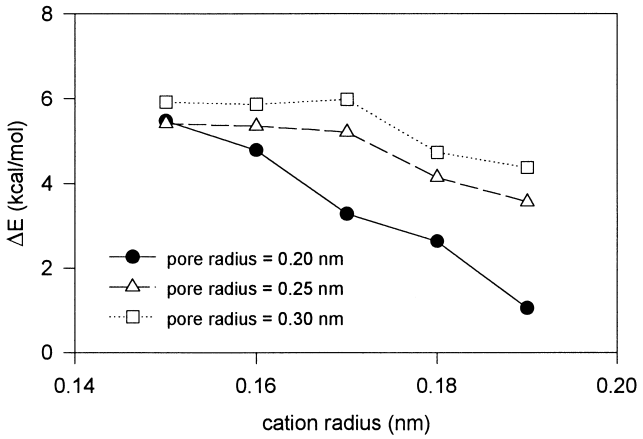

Fig. 8 The electrostatic solvation energy differences, ΔE, for cations are shown as a function of the cation cavity radius when the pore dielectric constant is changed from 78 to 5. The cation is located at three positions where the pore radius is 0.20, 0.25 and 0.30 nm

to the fitted quadratic curve, we suggest that the local pore dimensions play a more important role than the local charge distributions.

It may be argued that the above result is due to the uniform assignment of pore dielectric constant, whereas in fact the dielectric parameter inside the channel pore can not be a constant. It would be more accurate to consider the local dielectric constant to be determined by each distinct region inside the channel pore rather than to use an averaged dielectric constant. As discussed above, in the region where the pore dimensions are relatively large, the properties of pore water molecules would be more like those of bulk water. Therefore, the dielectric constant in this region would become larger and the calculated value of ΔE would be smaller. On the basis of this analysis, the dielectric effects of channel pore water molecules would be somewhat diminished when the local dielectric constant is taken into account, and the electrostatic solvation energy of the ion would be less sensitive to the dielectric constant of the pore water. However, according to our calculation, when the pore dielectric constant varies from 5 to 2.5, the trend of ΔE versus the local pore dimensions is similar to the case shown in Fig. 7.

In addition, we would like to point out that the effect of pore dielectric constant on the electrostatic solvation energy should strongly depend on the parameter of the ion radius. The Born radius corresponds to the size of the cavity formed by an ion in solvent (Rashin and Honig 1985). It is clear that the ion inside the narrow pores should have a different cavity radius compared to that in the wide pore. According to Roux et al. (1990), the Born radius of hydration can be interpreted in terms of the first peak in the solute-solvent radial distribution function. Thus, the Born radius is directly related to the properties of the solvent.

In order to explore the effect of the Born radius on the electrostatic energy, we have calculated the electrostatic solvation energies of cations with different radii for the cases where the pore dielectric constant is set to 78 and 5 using the FDPB method. Figure 8 shows the electrostatic solvation energy differences, ΔE, as a function of the cation radius when the pore dielectric constant decreases from 78 to 5 for three cases where the pore radii are 0.20, 0.25 and 0.30 nm, respectively. From Fig. 8, it is found that the value of ΔE for monovalent cations increases as the ion radius decreases. Meanwhile, the trend for the value of ΔE to be dependent on the pore radius as shown in Fig. 7 is still maintained. Since cations with a smaller ion radius have much stronger abilities to induce dielectric saturation, they should make the electrostatic solvation energy difference more dramatic than for larger cations when the pore dielectric constant decreases from 78 to 5.

Conclusions

The modified FDPB method for the aqueous channel pore has been used to study the dielectric effects of pore water on the electrostatic barrier. A model channel system that contains four α-helical segments with a right-handed twist is provided for this study. From the FDPB calculations, it is found that the effect of the pore dielectric constant on the electrostatic barrier of the permeating ion strongly depends on the pore radius in the vicinity of the ion. In the region where the pore radius is small, the pore dielectric constant can not significantly affect the barrier; this can be accounted for by the limited access of pore water molecules to the permeating ion. For this case, the ion electrostatic solvation energy is mostly defined by the interactions between the ion and the channel protein atoms. In contrast, the dielectric effect of pore water on the electrostatic barrier is quite strong for the wide domain where the interactions between ion and water are crucial and the variation of the electrostatic solvation energy become significant. Our results suggest that the electrostatic solvation energy of the permeating ion is dominated by local electrostatic interactions. Moreover, discussions of pore dielectric effects should be made with consideration of the particular dimensions of the channel pore.

We would like to point out that all calculations in this work were made on a model system. This study will be continued with other real or well-studied systems for which there are experimental and computational data as a reference.

Acknowledgements We thank Professor van Gunsteren for kindly providing us with the GROMOS package and for helpful comments on the initial version of this work. We also thank Dr. Smart for kindly sending us the HOLE program. This work was supported in part by the Chinese National High Technology project 863-103-13-03-01, the Chinese National Natural Science Foundation No. 39670187, and the Anhui Province Natural Science Foundation. All calculations were carried out on a Silicon Graphics Indy workstation and a Micro VAX 3500 computer at the Department of Biology in the University of Science and Technology of China.

Appendix

Here we present the detailed computational method for finding the radius of the defined cylinder in FDPB calculations. From the program HOLE, a series of spheres can be obtained, which accommodate the main portion of the channel pore without overlapping any channel protein atoms. We use (x_i, y_i, z_i) and r_i to represent the center and radius of these spheres, respectively; here i ranges from 1 to 80 for the current study. On the plane to which the pore axis is perpendicular and in which the sphere center is located, we can find the maximum distance R_i between the sphere center and the channel atoms. With the radius of R_i and the point (x_i, y_i, z_i), a series of new circles which cover the entire channel pore can be defined. The diameters of these circles D_x and D_y in the x and y directions can be calculated according to the following equations:

$$D_x = |P_{x2} - P_x| \tag{4}$$

and

$$D_y = |P_{y2} - P_{y1}|, \tag{5}$$

where P_{x2} and P_{y2} are the maximum coordinate values along the x and y axes, P_{x1} and P_{y1} are the minimum coordinate values. The radius of the cylinder, R_c, is defined as

$$R_c = 1/2\,[\mathrm{Max}\,(D_x, D_y)]. \tag{6}$$

Because the diameter of the α-helices is about 1 nm, the defined radius of the cylinder R_c is always within the range of the channel model. The cylinder with the radius R_c can accommodate the entire pore.

References

Berendsen HJC, Postma JPM, van Gunsteren WF, Hermans J (1981) Interaction models for water in relation to proteins hydration. In: Pullman B (ed) Intermolecular forces. Reidel, Dordrecht, pp 331–342

Berendsen HJC, Postma JPM, van Gunsteren WF, di Nola A, Haak JR (1984) Molecular dynamics with coupling to an external bath. J Chem Phys 81:3684–3690

Breed J, Sankararamakrishnan R, Kerr ID, Sansom MS (1996) Molecular dynamics simulations of water within models of ion channels. Biophys J 70:1643–1661

Chothia C, Levitt M, Richardson D (1977) Structure of proteins: packing of alpha-helices and pleated sheets. Proc Natl Acad Sci USA 74:4130–4134

Chothia C (1984) Principles that determine the structure of proteins. Annu Rev Biochem 53:537–572

Chou KC, Maggiora GM, Nemethy G, Scheraga HA (1988) Energetics of the structure of the four-a-helix bundle in proteins. Proc Natl Acad Sci USA 85:4295–4299

Daggett V, Kollman PA, Kuntz ID (1991) Molecular dynamics simulation of small peptides: dependence on dielectric model and PH. Biopolymers 31:285–304

Doak DG, Mulvey D, Kawaguchi K, Villalain J, Campell ID (1996) Structural studies of synthetic peptides dissected from the voltage-gated sodium channel. J Mol Biol 258:672–687

Gilson MK, Sharp KA, Honig BH (1987) Calculating the electrostatic potential of molecules in solution: method and error assessment. J Comp Chem 9:327–335

Greenblatt RE, Blatt Y, Montal M (1985) The Structure of the voltage-sensitive sodium channel. Inferences derived from computer-aided analysis of the electrophorus electricus channel primary structure. FEBS Lett 193:125–134

Gutman M, Tsfadia Y, Masad A, Nachiel E (1992) Quantitation of physico-chemical properties of the aqueous phase inside the phoE ionic channel. Biochim Biophys Acta 1109:141–148

Jordan PC (1986) Ion channel electrostatics and the shape of channel proteins. In: C. Miller (ed) Ion channel reconstitution. Plenum, New York, pp 37–55

Jordan PC, Bacquet RJ, McCammon JA, Tran P (1989) How electrolyte shielding influences the electrical potential in transmembrane ion channels. Biophys J 55:1041–1052

Kerr ID, Sankararamakrishnan R, Smart OS, Sansom MSP (1994) Parallel helix bundles and ion channels: molecular modeling via simulated annealing and restrained molecular dynamics. Biophys J 67:1501–1515

Kirkpatric S, Gelatt Jr CD, Vecchi MP (1983) Optimization by simulated annealing. Science 220:671–680

Levitt DG (1978) Electrostatic calculations for an ion channel. I. Energy and potential profiles and interaction between ions. Biophys J 22:202–219

Metropolis N, Rosenbluth AW, Rosenbluth MN, Teller AH, Teller E (1953) Equation of state calculations by fast computing machines. J Chem Phys 21:1087–1092

Montal M (1990) Molecular anatomy and molecular design of channel proteins. FASEB J 4:2623–2635

Nilges M, Brunger AT (1991) Automated modeling of coiled coils: application to the GCN4 dimerization region. Protein Eng 4:649–659

Noda M, Ikeda T, Kayano T, Suzuki H, Takeshima H, Kurasaki M, Takahashi H, Numa S (1986) Existence of distinct sodium channel messenger RNAs in rat brain. Nature 320:188–192

Oiki S, Danho W, Montal M (1988) Channel protein engineering: synthetic 22-mer peptide from the primary structure of the voltage-sensitive sodium channel forms ionic channels in lipid bilayers. Proc Natl Acad Sci USA 85:2393–2397

Parsegian A (1969) Energy of an ion crossing a low dielectric membrane: solution to four relevant electrostatic problems. Nature 221:844–846

Partenskii MB, Jordan PC (1992) Nonlinear dielectric behavior of water in transmembrane ion channels: ion energy barriers and the channel dielectric constant. J Phys Chem 96:3906–3910

Partenskii MB, Dorman V, Jordan PC (1994) Influence of a channel-forming peptide on energy barriers to ion permeation, viewed from a continuum dielectric perspective. Biophys J 67:1429–1438

Rashin AA, Honig B (1985) Reevaluation of the Born model of ion hydration. J Phys Chem 89:5588–5593

Richmond TJ, Richards FM (1978) Packing of alpha-helices: geometrical constraints and contact areas. J Mol Biol 119:537–555

Roux B, Yu H, Karplus M (1990) Molecular basis for the Born model of ion solvation. J Phys Chem 94:4683–4688

Ryckaert JP, Ciccotti G, Berendsen HJC (1977) Numerical integration of the Cartesian equations of motion of a system with constraints: molecular dynamics of n-Alkanes. J Comput Phys 23:327–341

Sansom MSP (1993) Structure and function of channel-forming peptaibols. Q Rev Biophys 26:365–421

Sansom MSP, Kerr ID (1993) Influenza virus M2 protein: a molecular modeling study of the ion channel. Protein Eng 6:65–74

Sharp KA, Honig B (1990) Electrostatic interactions in macromolecules: theory and application. Annu Rev Biophys Chem 19:302–332

Smart OS, Goodfellow JM, Wallace BA (1993) The pore dimensions of Gramicidin A. Biophys J 65:2455–2460

Stephan M, Agnew MS (1991) Voltage sensitive Na^+ channels: motifs, modes and modulation. Curr Opin Cell Biol 3:676–684

Treutlein HR, Lemmon MA, Engelmann DM, Brunger AT (1992) The glycophorin A transmembrane domain dimer: sequence-specific propensity for a right-handed supercoil of helices. Biochem 31:12726–12733

van Gunsteren WF, Berendsen HJC (1987) Groningen Molecular Simulation (GROMOS) Library Manual. Biomos, Nijenborgh 16, AG Groningen, The Netherlands